Reversible Deformation of Opal Elastomers

Benjamin Viel, Tilmann Ruhl, and Goetz P. Hellmann*

Deutsches Kunststoff-Institut (DKI, German Institute for Polymers), Darmstadt, Germany

Received October 30, 2006. Revised Manuscript Received August 31, 2007

Synthetic opals result from the crystallization of monodisperse silica or polymer beads of submicroscopic size. The beads self-organize to the face-centered cubic (fcc) lattice from which light is reflected wavelength selectively. At diameters of 0.15−0.3 μm, colors are singled out of white light by diffraction from the 111 plane of the lattice, the reflected color depending on the spacing a_{111}. With elastic opal films of core−shell (CS) beads, this spacing and, thereby, the color can be changed by deformation. This mechanochromic effect has so far been studied only on opals made of beads that were not chemically interconnected so the deformation was partly irreversible. In this study, opal films of polymeric core−shell beads were prepared by a melt-flow technique developed earlier in this institute. Afterward, the films were photo-cross-linked. They deformed indeed reversibly, however, with mechanical hysteresis effects. The strained fcc lattice causes a blue shift of the reflected color, which is indicative of a hard-sphere deformation mechanism. The shift is strong enough to switch monochromatic light on and off by only a few percent strain.

Introduction

In the past decade, colloidal crystals have attracted much attention for their optical properties. In particular, synthetic opals, with a face-centered cubic (fcc) lattice of submicroscopic inorganic or polymeric beads reminiscent of the natural gemstones,[1] have been prepared and characterized by various methods in this[2] and other laboratories.[3] These opals reflect UV, visible, or IR light wavelength selectively according to Braggs law. In systems with sufficient refractive contrast, the reflection peaks can widen to photonic band gaps.[4]

The colloidal-crystalline layers are commonly prepared from polymer latices or silica dispersions by colloidal self-assembly of the beads during appropriate drying. Layers from very soft and very hard beads, the two extremes, are indicated in Figure 1. Elastomeric beads, which are the basis of tire production, form compact elastic films (Figure 1a). The soft beads turn into polygons that merge into a continuous matrix. Yet, these films have a crystalline bead structure, as was revealed by scattering studies.[5] They are nonetheless transparent, for lack of optical contrast.

Hard polymer or silica beads crystallize similarly but do not deform (Figure 1b).[6] Consequently, the layers consist of two phases, the beads and the air around them which provides the contrast for color effects. Most studies on opals start from such layers which generally are prepared by horizontal or vertical deposition techniques.[3f−i] Due to their high porosity, unfortunately, very fragile layers result that, moreover, are often (but not always)[7] riven by many cracks that open due to shrinkage during drying.[8] Also, the drying technique is slow.

Natural opals are nonporous, due to a connecting matrix. To provide the synthetic opals with such a matrix, the pores can be infiltrated by monomers which then are polymerized (Figure 1c). Films thus obtained are compact and exhibit strength. Frequently, the beads were afterward removed to prepare inverse opals.[9] The original cracks are still present, in these films, in the form of defects.

* To whom correspondence should be addressed. Fax: (+49)6151/292855. Phone: (+49 6151/16-4506. E-mail: ghellmann@dki.tu-darmstadt.de.

(1) (a) Sanders, J. V. *Nature* **1964**, *204*, 1151. (b) Kinder, E. *Z. Phys.* **1969**, *224*, 74.

(2) (a) Ruhl, T.; Hellmann, G. P. *Macromol. Chem. Phys.* **2001**, *202*, 3502. (b) Ruhl, T.; Spahn, P.; Hellmann, G. P. *Polymer* **2003**, *44*, 7625. (c) Ruhl, T.; Spahn, P.; Winkler, H.; Hellmann, G. P. *Macromol. Chem. Phys.* **2004**, *205*, 1385. (d) Ruhl, T.; Spahn, P.; Winkler, H.; Hellmann, G. P. *Prog. Colloid Polym. Sci.* **2004**, *129*, 82. (e) Ruhl, T.; Spahn, P.; Hellmann, G. P.; Winkler, H. *Proc. SPIE: Photon. Cryst. Mater. Nanostruct.* **2004**, *5450*, 67. (f) Pursiainen, O. L. J.; Baumberg, J. J.; Ryan, K.; Bauer, J.; Winkler, H.; Viel, B.; Ruhl, T. *Appl. Phys. Lett* **2005**, *87*, 101902. (g) Ruhl, T.; Spahn, P.; Hermann, C.; Jamois, C.; Hess, O. *Adv. Funct. Mater.* **2006**, *16*, 885.

(3) (a) Jiang, P.; Ostojic, G. N.; Narat, R.; Mittleman, D. M.; Colvin, V. L. *Adv. Mater.* **2001**, *13*, 389. (b) Mayoral, R.; Requema, J.; Moya, J. S.; Lopez, C.; Cintas, A.; Miguez, H.; Meseguer, F.; Vazquez, L.; Holgado, M.; Blanco, A. *Adv. Mater.* **1997**, *9*, 257. (c) Park, S. H.; Gates, B.; Xia, Y. *Adv. Mater.* **1999**, *11*, 462, 466. (d) Egen, M.; Zentel, R. *Macromol. Chem. Phys.* **2004**, *205*, 1479. (e) Xia, Y.; Gates, B.; Yin, Y.; Lu, Y. *Adv. Mater.* **2000**, *12*, 693. (f) Griesebock, B.; Egen, M.; Zentel, R. *Chem. Mater.* **2002**, *14*, 4023. (g) Müller, M.; Zentel, R.; Maka, T.; Romanov, S. G.; Sotomayor Torres, C. M. *Chem. Mater.* **2000**, *12*, 2508. (h) Yan, O.; Zhou, Z.; Zhao, X. S. *Langmuir* **2005**, *21*, 3158. (i) Jiang, J. P.; Bertone, J. F.; Hwang, K. S.; Colvin, V. I. *Chem. Mater.* **1999**, *11*, 2132.

(4) (a) Yablonowitch, E. *Phys. Rev. Lett.* **1987**, *58*, 2059. (b) John, S. *Phys. Rev. Lett.* **1987**, *58*, 2486. (c) Joannopoulos, J. D.; Villeneuve, P. R.; Fan, S. *Nature* **1997**, *386*, 143.

(5) (a) Rieger, J.; Haedicke, E.; Ley, G.; Lindner, P. *Phys. Rev. Lett.* **1992**, *68*, 2782. (b) Men, Y.; Rieger, J.; Roth, S. V.; Gehrke, R.; Kong, X. *Langmuir* **2006**, *22*, 8285.

(6) Martelozzo, V. C.; Schofield, A. B.; Poon, W. C. K.; Pusey, P. N. *Phys. Rev. E* **2002**, *66*, 021408.

(7) (a) Wong, S.; Kitaev, V.; Ozin, G. A. *J. Am. Chem. Soc.* **2003**, *125*, 15590. (b) Jin, C.; McLachlan, M. A.; McComb, D. W.; De la Rue, R. M.; Johnson, N. P. *Nano Lett.* **2005**, *5*, 2646.

(8) Tirumkudulu, M. S.; Russel, W. B. *Langmuir* **2005**, *21*, 4938.

(9) (a) Arsenault, A. C.; Clark, T. J.; von Freymann, G.; Cademartiri, L.; Sapienza, R.; Bertolotti, J.; Vekris, E.; Wong, S.; Kitaev, V.; Manners, I.; Wang, R. Z.; John, S.; Wiersma, D.; Ozin, G. A. *Nat. Mater.* **2006**, *5*, 179. (b) Sumioka, K.; Kayashima, H.; Tsutsui, T. *Adv. Mater.* **2002**, *14*, 1284.

10.1021/cm062582a CCC: $37.00
Published on Web 10/24/2007

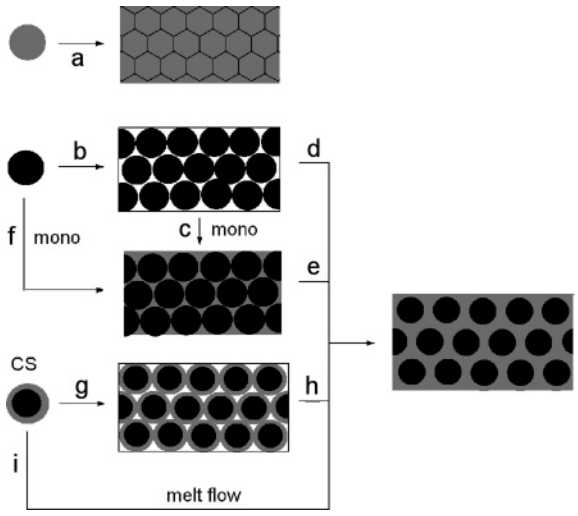

Figure 1. Colloidal crystals from soft (gray), hard (black), and hard−soft CS beads, prepared by various strategies: (a) filmification, (b,g) deposition from the dispersion, (c) polymerization, (d,e) swelling, (f) spin coating, (h) annealing, and (i) melt-flow technique.

Some more refined methods are illustrated in Figure 1 as well. Beads have been swollen on the outside with a solvent until they coalesced (Figure 1d),[10] or the matrix polymer was swollen (Figure 1e).[11] Starting from beads dispersed in a cross-linking monomer, silica−polymer hybrids have been prepared by spin-coating and polymerization (without cracks, Figure 1f).[12]

Two other strategies make use of core−shell (CS) beads. Nonporous opal films have been obtained by deposition from the dispersion (Figure 1g) and subsequent prolonged annealing (Figure 1h).[13] Similar products can be prepared faster by subjecting CS beads to melt flow, in a press or an extruder (Figure 1i). The self-organization is mainly driven by shear, as in the spin-coating technique in Figure 1f. This technique, which was introduced in ref 2a−c, is the basis of this report. It will be reviewed in the next section.

In the opal structure on the right in Figure 1, the beads are not in direct contact but separated by the matrix polymer. When this matrix is a soft elastomer, the opal films can be stretched considerably like rubbers or thermoplastic elastomers,[14] however, with special mechanochromic effects. Strain deforms the crystalline lattice as well so the reflected colors change. This effect, which suggests applications as deformation sensors and optical switches, is the topic of this paper.

The shear deformation of colloidal lattices has been investigated before, on ordered dispersions[15] and on simple

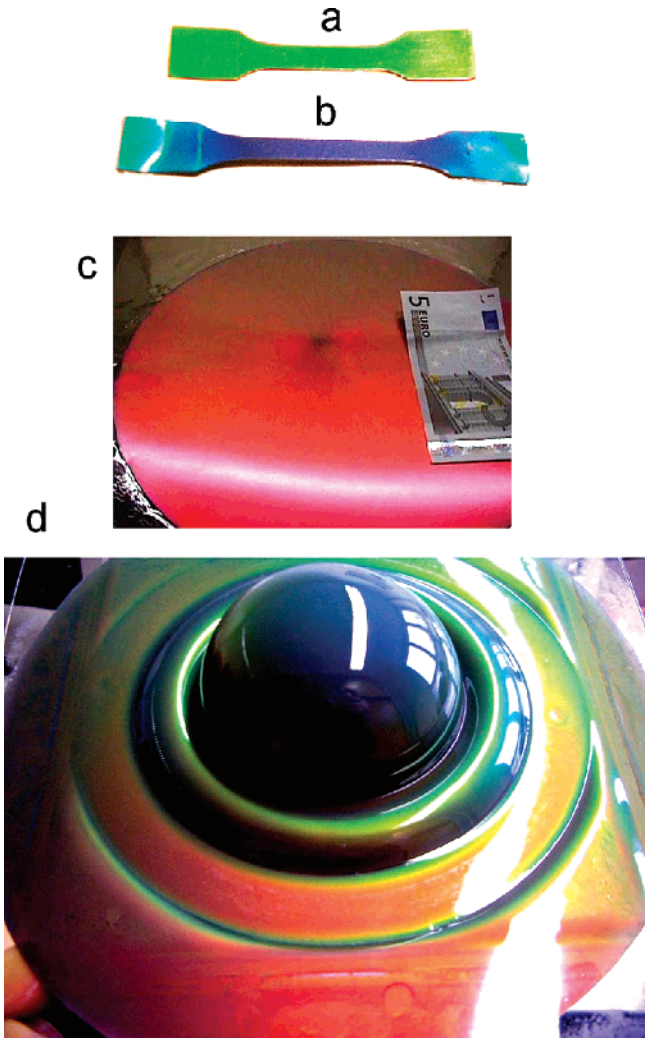

Figure 2. Elastomeric opal films: (a,b) test bars; (a) original; (b) strained to $\epsilon = 200\%$ and then released (residual deformation $\Delta\epsilon_\infty = 95\%$); (c,d) disk prepared by compression molding, (c) original and (d) deformed to a cup by deep drawing.

elastomeric latex films,[5] on polymer−polymer CS opals,[13d,e] and on silica−polymer opals made by infiltration.[11b] The beads were never chemically interconnected in the opals because either the matrix was not cross-linked or the beads were not linked to the matrix. Therefore, large strain led to slippage of crystalline layers and thus irreversible deformation.

In this study, the effects of interconnecting all beads by cross-linking were examined. Opal films were prepared from CS beads by our melt-flow technique. At first, the beads in these films were not tied together because, otherwise, there would have been no melt. But then the films were photo-cross-linked and a coherent bead network was created.

The mechanical and optical behavior of the un-cross-linked and cross-linked films will be discussed. To demonstrate the color effects, an un-cross-linked test bar is shown in Figure 2a,b, unstrained and strained-and-released. The green shifts to blue. In Figure 2c, an opal disk is shown under a polycarbonate sheet. This disk was deformed into the cup

(10) Rugge, A.; Ford, W. T.; Tolbert, S. H. *Langmuir* **2003**, *19*, 7852.
(11) (a) Fudouzi, H.; Sawada, T. *Langmuir* **2006**, *22*, 1365. (b) Jethmalani, J. M.; Ford, J. T. *Chem. Mater.* **1996**, *8*, 2138.
(12) Jiang, P.; McFarland, M. J. *J. Am. Chem. Soc.* **2004**, *126*, 13778.
(13) (a) Kumacheva, E.; Kalinina, O.; Lilge, L. *Adv. Mater.* **1999**, *11*, 231. (b) Rupaner, R.; Leyrer, R.; Schurmacher, P. BASF, Patent DE 198 20 302, 2000. (c) He, X.; Thomann, Y.; Leyrer, R. J.; Rieger, J. *Polym. Bull.* **2006**, *57*, 785. (d) Fava, D.; Fau, Y. S.; Kumacheva, E.; Winnik, M. A.; Shinozaki, D. M. *Macromolecules* **2006**, *39*, 1665. (e) Lepizzera, S.; Pith, T.; Fond, C.; Lambla, M. *Macromolecules* **1997**, *30*, 7945.
(14) (a) Holden, G.; Legge, N. R.; Quirk, R.; Schroeder, H. E. *Thermoplastic Elastomers, 2nd Ed.*; Hanser: Munich, 1996. (b) Staudinger, U.; Weidisch, R.; Zhu, Y.; Gido, S. P.; Uhrig, D.; Mays, J. W.; Iatrou, H.; Hadjichristidis, N. *Macromol. Symp.* **2006**, *233*, 42.
(15) (a) Ackerson, B. J.; Clark, N. A. *Phys. Rev. Lett.* **1981**, *46*, 123. (b) Weiss, J. A.; Oxtoby, D. W.; Grier, D. G.; Murray, C. A. *J. Chem. Phys.* **1995**, *103*, 1180.

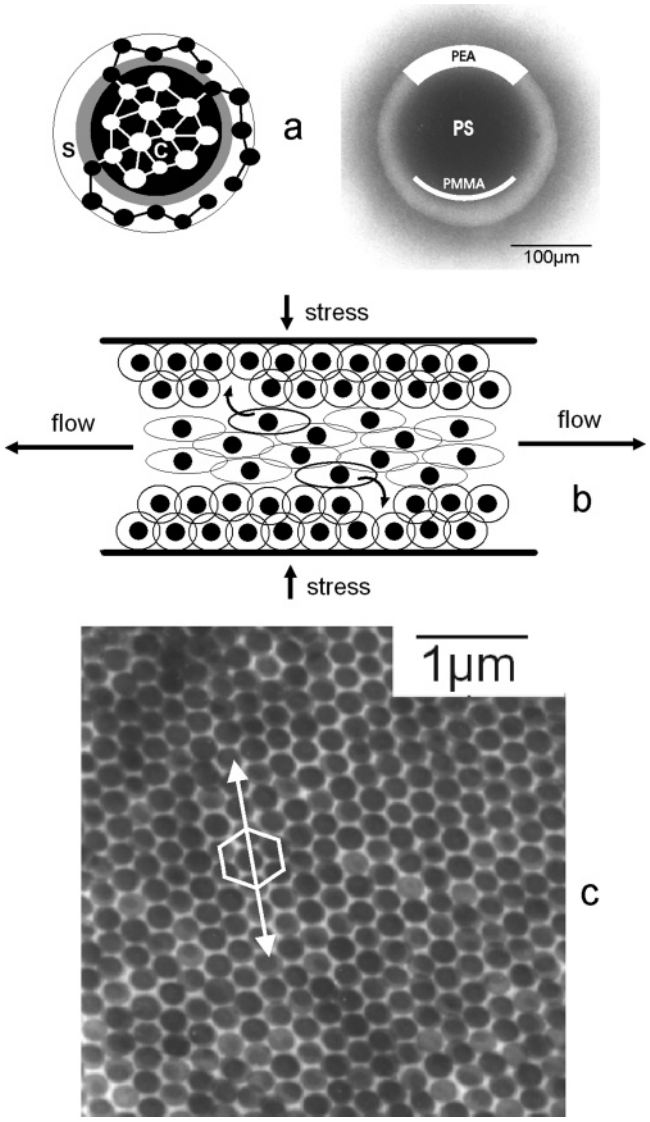

Figure 3. CS beads: (a) scheme of the architecture and TEM image; (b) ordering by melt flow (horizontal) under stress (vertical) in a press; (c) hexagonal layer of beads parallel to the film surface with the arrow pointing into the radial direction of the disk.

in Figure 2d. The red turns to all colors of the rainbow, owing to the angle and strain dependence of the reflected color.

Experimental Section

The preparation methods have been outlined in detail before.[2b,c] Beads with the architecture in Figure 3a were synthesized by emulsion polymerization. They are core−interlayer−shell beads. The core consists of polystyrene (PS), cross-linked with butanediol diacrylate (BDDA, 3 mol %), and the thin interlayer of polymethylmethacrylate (PMMA), cross-linked with allylmethacrylate (ALMA, 10 mol %). The shell is made of polyethylacrylate (PEA), not cross-linked but grafted to the interlayer: the ALMA in the PMMA interlayer guarantees a high degree of grafting, about $^2/_3$ of all PEA chains being tied to the interlayer. All three microphases in the beads are thus interconnected. The composition was $PS_{30}ciPMMA_{13}$-$isPEA_{57}$ by weight.

These beads are of the hard−soft type, with a rigid PS−PMMA core and a soft, deformable PEA shell. Owing to this shell, the product was a tacky mass. The TEM image in Figure 3a of a bead deposited on a grid illustrates the architecture. The bead diameter, overall 230 nm, grows with each microphase as 66 + 9 + 25%, meaning that the rigid core accounts for $^3/_4$ of the total diameter.

After extrusion of the elastomeric mass, opal films were prepared from it at 130 °C in a press (Dr. Collin GmbH; Typ 300E). The mass was placed between the plates of the press, in the center, and then stress was applied. The mass was allowed to flow radially outward as shown in Figure 3b. In this process, beads are constantly being deposited along the plates, forming crystalline layers of the 111 plane, one on top of the other, in the characteristic ABC sequence of the fcc lattice. In the TEM image in Figure 3c, the hexagonally arranged PS cores are shown. They seem to touch but are separated by the shells forming the matrix. While the melt flow lasts, the opaline lattice grows inward, layer-by-layer, from the plates toward the center. The flowing center of the film becomes steadily thinner and the stress increases until, eventually, the melt flow stops.

This technique is fast and suited for series production of large or small, thin or thick films, free or on substrates. A big advantage is that since the melt flow is radially directed, the fcc lattice is macroscopically oriented. In disks as in Figure 2c, the hexagons of the 111 plane point radially outward as indicated by the arrow in Figure 3c. Each radial sector of the disks is a monodomain. There is no multicrystallinity. But the technique has also a shortcoming: the crystalline layers below both film surfaces account only for about $^2/_3$ of the total thickness while $^1/_3$, in the film center, remains disordered.[2b]

To prepare photo-cross-linkable opal disks, the CS beads were mixed at 120 °C in a microextruder (micro 1, DSM-Research) with 1−5 wt % of benzophenone (BP). The carbonyl function in BP is activated by light[16] and generates on the polymer chains carbon radicals that combine to branches and cross-links.[17] To cross-link the opal disks containing BP, they were irradiated for 5−15 min with a high-pressure tungsten lamp (Osram Ultravitalux 300 W).

Stress−strain curves were recorded with dog-bone test bars that had been cut from the opal disks along the radial direction. Therefore, the drawing direction coincides with the arrow in Figure 3c. For the mechanical tests, a tensile tester (Zwick Z020 TH2A) was used, either in strain tests to rupture or in cyclic tests.

The film structure was investigated using ultrathin sections, contrasted with RuO_4, in a transmission electron microscope (Zeiss 90950). The surface structure was analyzed using an atomic force microscope ((Veeco CP II) in the contact mode. Spectra were recorded with a UV−vis spectrometer (Perkin-Elmer Lambda 40). Rectangular film samples were drawn in the spectrometer using a self-made device with clamps and a screw. The strain was measured with a gauge.

Results and Discussion

Every single CS bead, with its cross-linked core and grafted shell, can be viewed as practically one giant molecule. Consequently, very little of the photo-cross-linker BP should have sufficed to cross-link an entire opal film: two cross-links on each bead should have been enough, which translates into ppm of BP needed. Instead, it turned out that a few percent of BP was necessary to bring about satisfactory cross-linking. Obviously, the cross-linking was not very efficient.

(16) Allmer, K.; Hult, A.; Ranby, B. *J. Polym. Sci., Part A: Polym. Chem.* **1989**, *27*, 1641.
(17) (a) Millan, M.; Park, M.; Patton, D.; Locklin, J.; Deng, S.; Advincula, R. *Polym. Prepr.* **2004**, *45*, 937. (b) Prucker, O.; Naumann, C. A.; Rühe, J.; Knoll, W.; Frank, C. W. *J. Am. Chem. Soc.* **1999**, *121*, 8766.

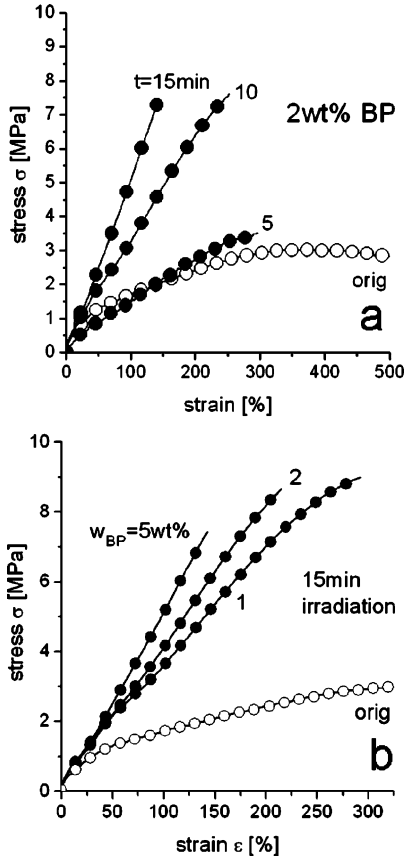

Figure 4. Stress−strain curves of un-cross-linked (orig) and cross-linked opal films: (a) 2 wt % BP, various irradiation times; (b) 15 min irradiation time, various BP contents (orig: original, un-cross-linked film).

Stress−strain curves are shown in Figure 4 for films without and with BP. The un-cross-linked film can be drawn almost infinitely. But after a maximum at $\epsilon \cong 380\%$, the stress drops steadily, due to flow. This film is in fact not an elastomer but a very viscous liquid. The BP-modified, cross-linked films, on the contrary, show the monotonous stress−strain curves expected from elastomers. Prolonged irradiation stiffens the films (Figure 4a), as does an increased BP content (Figure 4b). Compared to commercial rubbers, these films are quite stiff, almost leathery.

The reversibility of deformation was examined with draw-and-release cycles with an end strain of $\epsilon_{mqx} = 200\%$. In un-cross-linked films, the strain was largely irreversible. The film in Figure 2b retained about half of its deformation after release. Curves from a cross-linked film are shown in Figure 5. The first drawing curve (1up) in Figure 5a is linear but the release curve (1down) is bent, far below the drawing curve. Since the areas under the two curves represent the mechanical energies A_{up} and A_{down}, the difference between them yields the heat production in the cycle, which is known as the mechanical hysteresis:

$$Q = A_{up} - A_{down} = \int(\sigma_{up} - \sigma_{down})\, d\epsilon \qquad (1)$$

This hysteresis is strong, in the first cycle. Moreover, the release curve returns to the stress-free level ($\sigma = 0$) not at $\epsilon = 0$, as it would have with a perfect rubber, but at a high residual strain of $\Delta\epsilon_0 = 76\%$. This seems to indicate insufficient elasticity, despite the cross-linking.

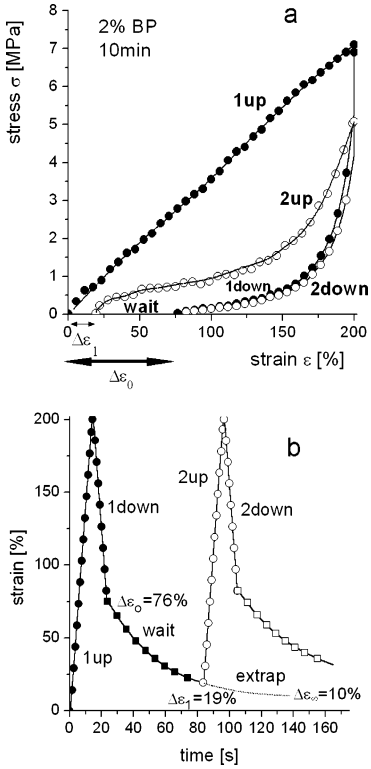

Figure 5. Two hysteresis cycles (up−down), separated by a waiting period (wait) of the opal film cross-linked with 2 wt % BP (10 min irradiation): (a) stress−strain diagram; (b) strain−time diagram, $\Delta\epsilon$: residual strain.

However, the residual deformation proved to be only transitory. It decreased in time. The second drawing curve (2up) in Figure 5a does not start at $\Delta\epsilon_0$ but at the much smaller strain $\Delta\epsilon_1 = 19\%$ because the two cycles were separated by a period (wait) of 1 min. What happened in this minute is shown in Figure 5b: the residual strain $\Delta\epsilon$ decreases exponentially to $\Delta\epsilon_1$, where the second cycle starts, and is extrapolated to drop eventually to a small final strain of $\Delta\epsilon_\infty = 10\%$. This means that almost the original opal structure was regained. The recovery is only delayed because the molecular relaxations in the film are slow. Taking into account that these elastomeric films are highly filled, containing 43 wt % of rigid cores, slow relaxation is not at all surprising.

The second draw-and-release cycle in Figure 5a is more rubber-like, with little hysteresis. The overall pattern of curves in Figure 5 is reminiscent of high-quality thermoplastic elastomers.[14]

As demonstrated in Figure 2, strain causes a blue shift of the reflected color (notice that the cup in Figure 2d is red as in Figure 2c in the foreground, but blue on the top, although the viewing angles are equal: this is a strain effect).

Unstrained and strained test bars were analyzed by UV−vis spectroscopy in transmission, at normal irradiation ($\theta = 0°$). The spectra of un-cross-linked and cross-linked films are compiled in Figure 6. All curves feature a Bragg peak due to the reflection from the 111 plane of the fcc lattice and, at shorter wavelengths, a plateau caused by diffuse scattering from the disordered center of the films. The peak and the plateau both travel under increasing strain to shorter wavelengths.

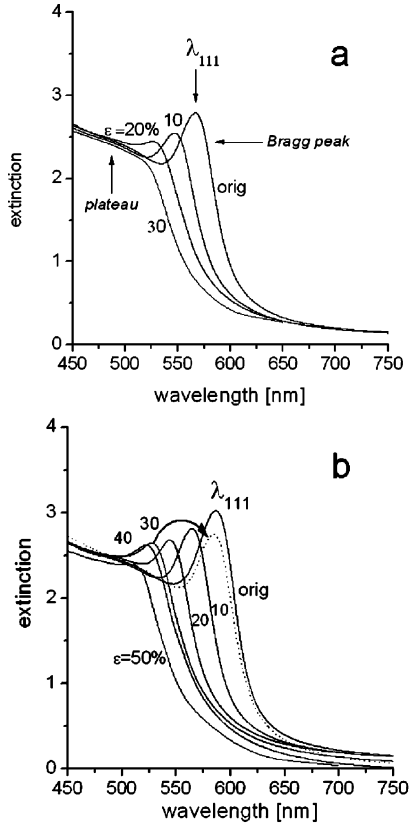

Figure 6. UV−vis spectra of original and drawn opal films: (a) un-cross-linked, (b) cross-linked (2 wt % PB, 10 min irradiation), ϵ: elongation, λ_{111}: Bragg peak, dashed curve in (b): spectrum after releasing the test bar drawn to $\epsilon = 30\%$.

The Bragg peak appears in the undrawn film at the wavelength

$$\lambda_{111} = 2na_{111} \tag{2}$$

where n is the average refractive index of the film and a_{111} the layer spacing of the 111 plane which depends on the bead-to-bead distance d as (Figure 7a)

$$a_{111} = d\sqrt{\frac{2}{3}} \tag{3}$$

Horizontal strain causes the spacing a_{111} to decrease to a smaller $a(\epsilon)$ (Figure 7b). This explains the blue shift of the color upon drawing. Interestingly, this shift is similar for the un-cross-linked and cross-linked film. The lattice deformation is evidently similar. This is owed to the effect of chain entanglements which, at small strains $\epsilon \leq 30\%$ and over short times, can replace cross-links. The difference in elasticity between the two films became apparent only when the test bars were held under strain for prolonged times. After release, the un-cross-linked bar stayed deformed while the cross-linked bar came back to almost its original dimensions and color. This is demonstrated in Figure 6b for a strain of $\epsilon = 30\%$. The strained-and-released test bar yielded, after holding it for 15 min at $\epsilon = 30\%$ before release, practically the same UV−vis curve as the original bar.

The shift of the spacing $a(\epsilon)$, calculated from Figure 6b with eq 2 and shown in Figure 8a, is informative because it elucidates the deformation mechanism. The decrease of $a(\epsilon)$

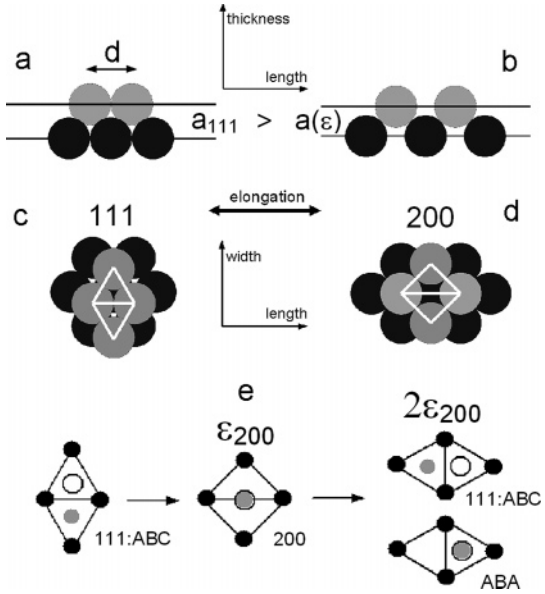

Figure 7. Spheres in the fcc lattice, viewed (a,b) edge-on and (c,d) from above: (a,c) original, (b,d) horizontally elongated; (e) large deformation to strains ϵ_{200} (eq 5) and $2\epsilon_{200}$: three layers of the lattice with gray spheres in the top, black spheres in the middle, and white spheres in the bottom layer.

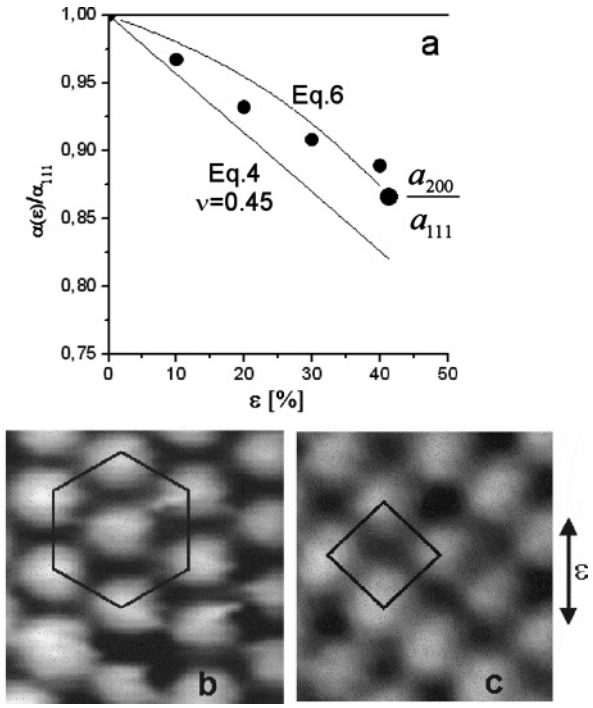

Figure 8. Lattice deformation: (a) layer spacing $a(\epsilon)$ from Figure 6b (with eq 2) and calculated model curves (with eq 4 and eq 6); (b,c) electron micrographs of layers parallel to the surface, (b) in the original film, (c) after drawing to the strain ϵ_{200}.

can be interpreted using two extreme models, one for homogeneous matrices and one for arrays of hard spheres.

A homogeneous polymer film will be elongated by a strain ϵ by the factor $(1 + \epsilon)$, and the film thickness will simultaneously decrease by $(1 - \nu\epsilon)$, ν being the Poisson ratio. The change in the spacing $a(\epsilon)$ of the 111 plane should equal the thickness change:

$$\frac{a(\epsilon)}{a_{111}} = \frac{\lambda(\epsilon)}{\lambda_{111}} = 1 - \nu\epsilon \tag{4}$$

But this equation fits the data in Figure 8a only with an unrealistic Poisson ratio of $\nu \cong 0.28$. Therefore, a curve is shown in the figure that was calculated with a Poisson ratio of $\nu \cong 0.45$ which seems realistic because $\nu \cong 0.4$ is normal for hard polymers (the cores) and $\nu \cong 0.5$ for soft elastomers (the shells). Evidently, however, this curve overestimates the actual decrease of $a(\epsilon)$, and for a good reason: the homogeneous deformation mechanism, on the local level, would call for an interpenetration of the rigid bead cores which is impossible.

The alternative model for hard spheres avoids this interpenetration. The spheres move under strain as shown in Figure 7: horizontal elongation deforms the rhombus in Figure 7c until, at the strain

$$1 + \epsilon_{200} = \sqrt{2} \tag{5}$$

it turns into the square in Figure 7d. The four beads in Figure 7c,d always stay in closest contact. Monolayer deformations of this type have been shown impressively in 2D studies.[18] Assuming that, under strain, adjacent 111 layers also keep in closest contact (Figure 7a,b), the lattice deformation can be calculated. The 111 spacing should change as

$$\frac{a(\epsilon)}{a_{111}} = \sqrt{\frac{3}{2}\left(1 - \frac{1}{4 - (1+\epsilon)^2}\right)}$$
$$\frac{a_{200}}{a_{111}} = \frac{a(\epsilon_{200})}{a_{111}} = \sqrt{\frac{3}{4}} \tag{6}$$

As shown in Figure 8a, this equation yields a better description. It underestimates the measured decrease of $a(\epsilon)$, but that should be due to the deformability of the soft shells of these CS beads.

Two effects support this deformation model of an array of more or less rigid beads. The first is shown in the AFM images in Figure 8b,c. At $\epsilon \cong 40\%$, as predicted by Figure 7c,d, the hexagons of the 111 plane are rearranged to squares. Approximately at this strain, at ϵ_{200} of eq 5, the fcc lattice is oriented such that no longer the 111 plane but the 200 plane extends parallel to the film surface. The lattice is in this state actually not strained but only rearranged. It would be in equilibrium if it were not for the cross-links. But naturally, the network of the cross-links remembers the original dimensions so the drawn film shrank back when released.

The second effect mentioned above is that, in UV−vis spectra measured in transmission, no cross-linked film ever exhibited a Bragg peak at higher strains than $\epsilon > 40\%$. Attempts at improving the lattice quality in test bars by annealing them at elevated temperatures or swelling them in various media failed consistently. AFM images always revealed disordered bead arrays.

Apparently, there is no crystal beyond the deformation ϵ_{200}. In literature studies, crystalline order was still found at higher strains,[11b,13a,e] but in those, the beads were not interconnected. Layers were found to slip, which cannot happen in cross-linked films.

In Figure 7e, an effect is indicated that may be an initiator of disorder. A rhombus of the 111 plane is shown, and one bead either above or below it, according to the ABC sequence of the fcc lattice. At the strain ϵ_{200}, the outer beads move into the center of the square. So far, this is a controlled conversion of the 111 to the 200 plane. But then the disorder begins. Doubling the strain should lead again to a rhombus, now horizontal. But the two beads above and below it have a choice: they can either move into the same or into different triangles, establishing an ABC or an ABA sequence. When the two change at random, the three-dimensional order of the crystal is lost.

Actually, this ABC−ABA switching should not disturb the order in the thickness direction. There should still be stacks of hexagonal bead layers parallel to the film surface. But the switching may well be accompanied by layer distortion, which causes general disorder. It certainly seems as though the strain ϵ_{200} marks the upper limit for the existence of the crystal.

The disorder above ϵ_{200} is not permanent. It is reversible since the cross-links bring any deformed structure reliably back to the original. Therefore, the films can be switched from order to disorder and back by high strains. But small strains below ϵ_{200}, where the order is upheld, should suffice in practice. Deformation sensors need switching from dark to light at a constant wavelength. According to Figure 6b, this calls only for small deformations: a strain of $\epsilon = 10\%$ shifts the Bragg peak already out of the range of the original peak. Even $\epsilon < 10\%$ suffice for the construction of a light−dark switch.

In a final note, the question of the colors at high strains is addressed. When the films were elongated way beyond ϵ_{200}, their color became somewhat less intense but did not disappear. The films turned blue and then violet, although there was no Bragg peak anymore. It is the plateau in Figure 6, caused by disordered regions in the films, that produces the colors at high strains. This plateau has an upper edge that undergoes a blue shift just like the Bragg peak because strain distorts ordered and disordered bead arrays similarly. At wavelengths <500 nm, not far from the UV border, the plateau is, in its optical consequences, not much different from a peak: it takes away part of the visible spectrum so the complementary color is seen.

Conclusion

Synthetic opals were prepared from polymeric core−shell (CS) beads by a fast melt-flow technique that permits the large-scale, large-area production of films. These films were afterward photo-cross-linked. Since the core of the beads was rigid but the shell elastomeric, the films could be strained considerably. The deformation proved to be almost reversible. The fcc lattice of the beads deformed under strain $\epsilon < 40\%$, as expected for beads with a big rigid core. At $\epsilon > 40\%$, the crystalline order was lost but was restored after release. The deformation caused a strong blue shift of the

(18) Zhu, M.; Li, Y.; Meng, T.; Zhan, P.; Sun, J.; Wu, J.; Wang, Z.; Zhu, S.; Ming, N. *Langmuir* **2006**, *22*, 7248.

reflected color. Monochromatic light of the appropriate wavelength can be switched from light to dark by only a few percent strain, which makes these films suited as deformation sensors. However, the films are not yet suited for applications where many strain-and-release cycles in fast sequence are desired. Since the rigid core in the beads is so big, the films are quite stiff, and relaxations in them are relatively slow. It took minutes before a strained film recovered its original dimensions. Work on softer films with a lower core−shell ratio is in progress.

Acknowledgment. The authors thank Merck KGaA (Darmstadt, Germany) and the Bundesministerium für Bildung und Forschung (BMBF project 13N8275, *KODO*) for financial support.

CM062582A